

**NANO EXPRESS**

**Open Access**

# Fabrication of Si heterojunction solar cells using P-doped Si nanocrystals embedded in $\text{SiN}_x$ films as emitters

Ping-Jung Wu, Yu-Cian Wang and I-Chen Chen<sup>\*</sup>

## Abstract

Si heterojunction solar cells were fabricated on p-type single-crystal Si (sc-Si) substrates using phosphorus-doped Si nanocrystals (Si-NCs) embedded in  $\text{SiN}_x$  ( $\text{Si-NCs/SiN}_x$ ) films as emitters. The Si-NCs were formed by post-annealing of silicon-rich silicon nitride films deposited by electron cyclotron resonance chemical vapor deposition. We investigate the influence of the N/Si ratio in the  $\text{Si-NCs/SiN}_x$  films on their electrical and optical properties, as well as the photovoltaic properties of the fabricated heterojunction devices. Increasing the nitrogen content enhances the optical gap  $E_{\text{g}}$  while deteriorating the electrical conductivity of the  $\text{Si-NCs/SiN}_x$  film, leading to an increased short-circuit current density and a decreased fill factor of the heterojunction device. These trends could be interpreted by a bi-phase model which describes the  $\text{Si-NCs/SiN}_x$  film as a mixture of a high-transparency  $\text{SiN}_x$  phase and a low-resistivity Si-NC phase. A preliminary efficiency of 8.6% is achieved for the  $\text{Si-NCs/sc-Si}$  heterojunction solar cell.

**Keywords:** Si nanocrystals; Heterojunction solar cells; Emitter

## Background

Materials consisting of silicon nanocrystals (Si-NCs) embedded in a dielectric matrix are one promising candidate to realize Si-based third-generation photovoltaic devices owing to their potential benefits of utilizing the visible light of terrestrial solar spectrum and overcoming the efficiency limit of crystalline Si (c-Si) solar cells [1-5]. Sub-stoichiometric Si-based dielectric materials, such as  $\text{SiO}_x$ ,  $\text{SiN}_x$ , and  $\text{SiC}_x$ , have been investigated for synthesis of Si-NCs [6-11]. The formation of Si-NCs is based on phase segregation and crystallization in Si-rich dielectric films during the post-annealing process [12].

The low conductivity of Si-NCs embedded in dielectric films limits their applications for the manufacturing of optoelectronic devices. For this reason, impurity doping in Si-NCs embedded in  $\text{SiO}_2$  has been demonstrated to modify the electrical properties of the layers, although there is some debate about the feasibility of doping in Si-NCs [13,14]. In addition to impurity doping, the choice of the surrounding dielectric matrix also plays a crucial role in charge carrier transport. Although the

formation of Si-NCs in the  $\text{SiO}_2$  matrix has been investigated in detail [12,15], the carrier transport ability in the Si-NC network is generally insufficient due to the large energy barrier of the surrounding oxide matrix. Charge carrier transport through narrower bandgap dielectrics, such as  $\text{Si}_3\text{N}_4$  or  $\text{SiC}$ , seems to be more feasible. Compared with  $\text{SiO}_2$  and  $\text{SiC}$ ,  $\text{Si}_3\text{N}_4$  may offer a compromise as a dielectric matrix for the Si-NC network used in solar cell applications since it possesses a medium bandgap (approximately 5.3 eV) which could reduce the energy barrier for carrier transport and also effectively avoid parasitic absorption. However, doped Si-NCs embedded in a  $\text{SiN}_x$  matrix ( $\text{Si-NCs/SiN}_x$ ) have not received much attention.

In this work, we present initial fabrication and characterization results of Si heterojunction solar cells using P-doped Si-NCs/ $\text{SiN}_x$  films as emitters. The P-doped Si-NCs/ $\text{SiN}_x$  films were prepared by electron cyclotron resonance chemical vapor deposition (ECR-CVD) followed by high-temperature annealing, and the influence of the chemical composition (N/Si ratio) on their physical properties was investigated. The photovoltaic properties of the fabricated heterojunction devices were

\* Correspondence: ichen@ncu.edu.tw  
Institute of Materials Science and Engineering, National Central University, Jhongli 320, Taiwan

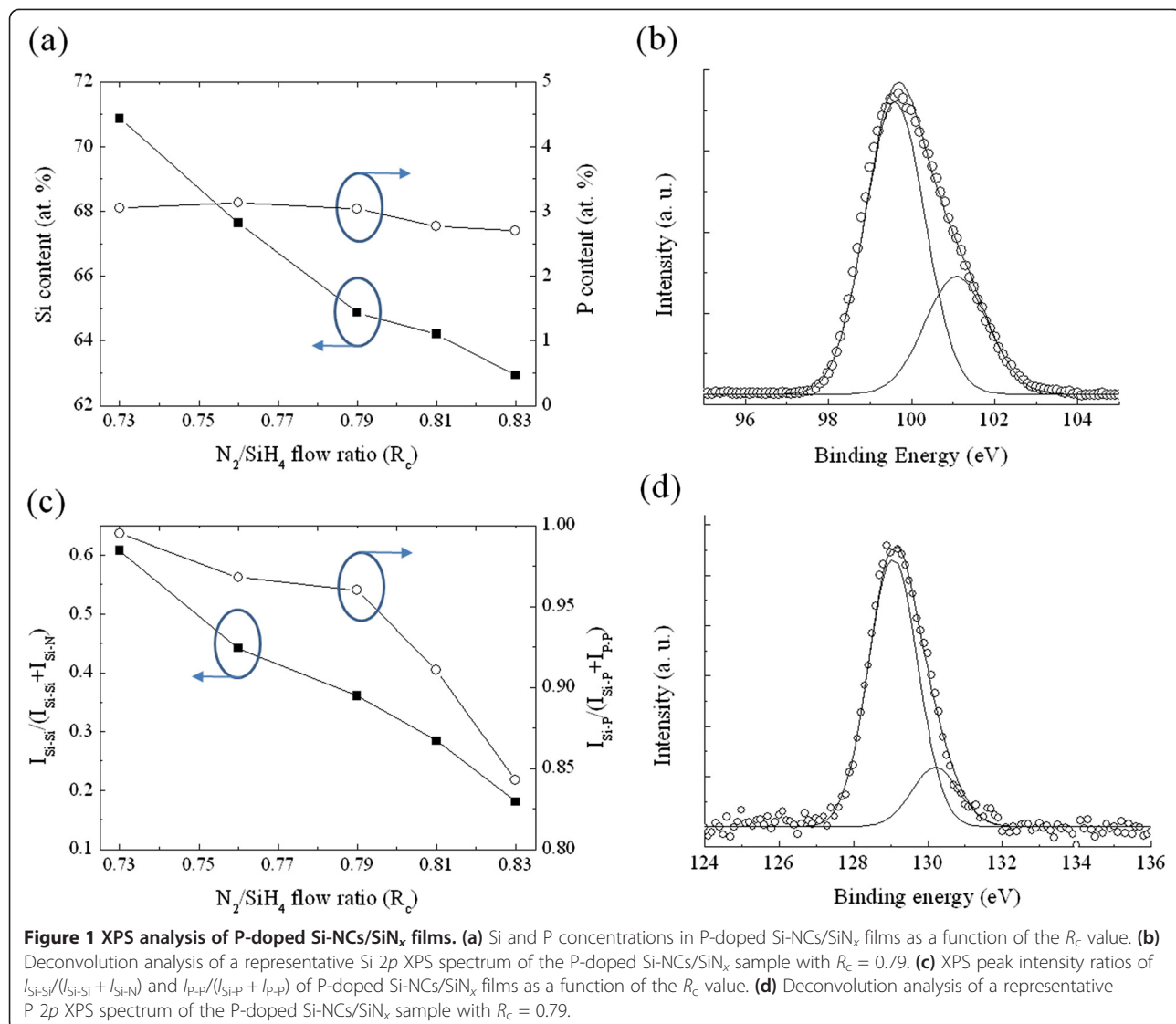


**Figure 1** XPS analysis of P-doped Si-NCs/SiN<sub>x</sub> films. **(a)** Si and P concentrations in P-doped Si-NCs/SiN<sub>x</sub> films as a function of the  $R_c$  value. **(b)** Deconvolution analysis of a representative Si 2p XPS spectrum of the P-doped Si-NCs/SiN<sub>x</sub> sample with  $R_c = 0.79$ . **(c)** XPS peak intensity ratios of  $I_{Si-Si}/(I_{Si-Si} + I_{Si-N})$  and  $I_{P-P}/(I_{Si-P} + I_{P-P})$  of P-doped Si-NCs/SiN<sub>x</sub> films as a function of the  $R_c$  value. **(d)** Deconvolution analysis of a representative P 2p XPS spectrum of the P-doped Si-NCs/SiN<sub>x</sub> sample with  $R_c = 0.79$ .

also examined as a function of the N/Si composition ratio in the P-doped Si-NCs/SiN<sub>x</sub> films.

## Methods

Fifty-nanometer-thick, homogeneous Si-rich silicon nitride (SRN) films containing phosphorus were deposited by a homemade ECRCVD system on single-side polished p-type (100) single crystalline Si (sc-Si) substrates with a thickness of 675 μm and a resistivity in the range of 5 to 20 Ω cm. Before placing into the deposition chamber, Si substrates were cleaned with acetone and rinsed in deionized water followed by removal of native oxide on Si wafers using a diluted HF dip (5%). The mixed SiH<sub>4</sub>, N<sub>2</sub>, Ar, and PH<sub>3</sub> gases were then introduced into the deposition chamber at 10 mTorr for film growth. The applied microwave power and the substrate temperature were kept on 700 W and 200°C, respectively. In order to study

the influence of the Si/N ratio on film properties, both SiH<sub>4</sub> and PH<sub>3</sub> flow rates were kept constant during film growth, while the gas mix ratio ( $R_c$ ) defined as  $N_2/SiH_4$  was varied in the range  $0.73 \leq R_c \leq 0.83$ . The formation of Si-NCs in as-deposited SRN films was carried out by post-growth annealing in a quartz tube furnace at 950°C in N<sub>2</sub> ambient. Samples with a 1 cm × 1 cm area were used for subsequent fabrication of heterojunction solar cells. Aluminum films deposited by electron gun evaporation were used as contact electrode layers in the solar cells. The front contact on top of the Si-NCs/SiN<sub>x</sub> film was defined by a shadow mask during Al deposition, while the rear contact covered the full back area of the cell. After metallization, the samples were heated at 500°C for 3 min to improve the electrical properties of the contacts.

For the characterization, the bonding configurations of the Si-NCs/SiN<sub>x</sub> films were identified by X-ray

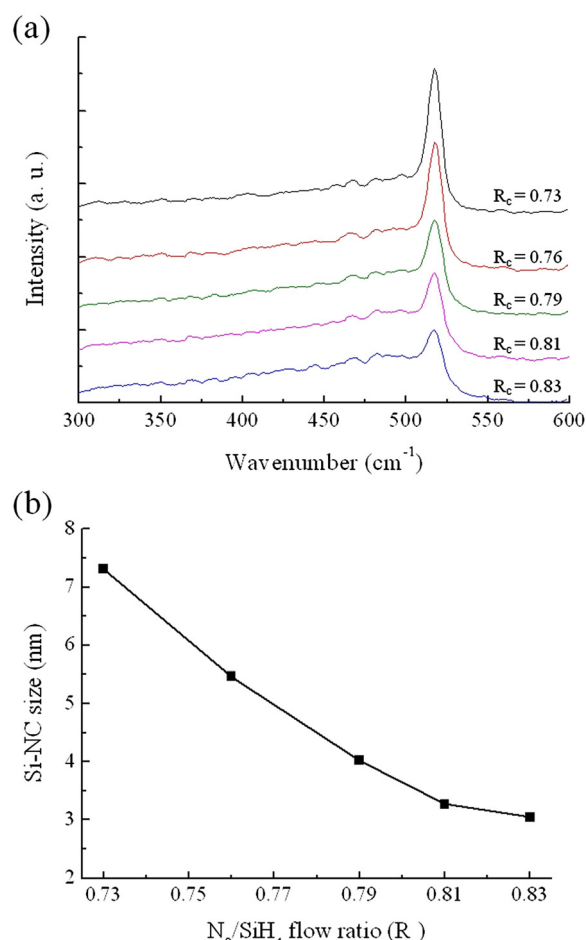


**Figure 2 Analysis of the crystallization behavior of P-doped Si-NCs/Si<sub>x</sub> films. (a)** Raman spectra of P-doped Si-NCs/Si<sub>x</sub> films with various  $R_c$  values. **(b)** Average Si-NC size of the Si-NCs/Si<sub>x</sub> film as a function of the  $R_c$  value obtained by XRD data with the Scherrer equation.

photoelectron spectroscopy (XPS). Micro-Raman spectroscopy and transmission electron microscopy (TEM) were used to investigate the crystallization behavior in SRN films after post-growth annealing. Fused quartz wafers were used as substrates for Raman studies to avoid the signal contribution from Si substrates during Raman measurements. X-ray diffraction (XRD) was used to evaluate the Si-NC size of annealed samples. The photovoltaic properties of the fabricated heterojunction solar cells were evaluated at room temperature based on the illuminated current density versus voltage ( $J-V$ ) and the internal quantum efficiency (IQE) characteristics under 1-sun air mass 1.5 global spectrum.

## Results and discussion

The relative elemental composition of the P-doped Si-NCs/Si<sub>x</sub> films was estimated from XPS spectra. The calculation of the chemical composition is based

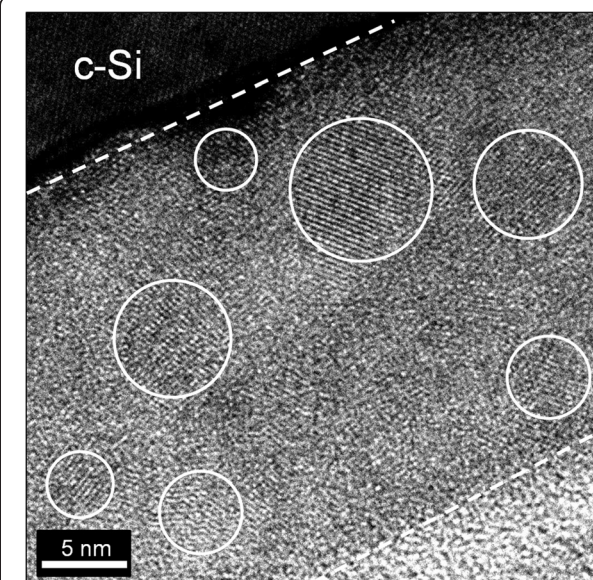
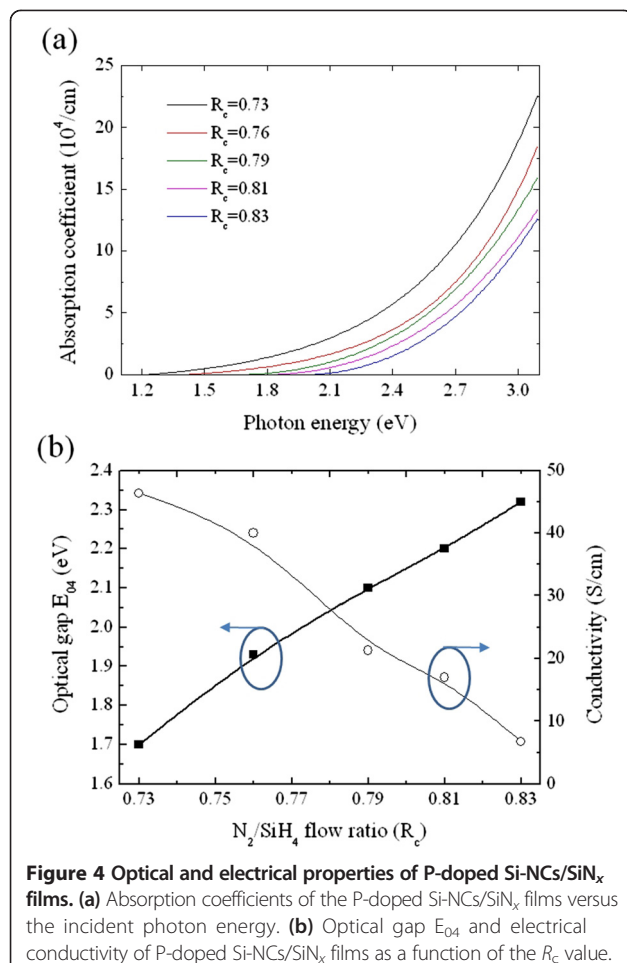


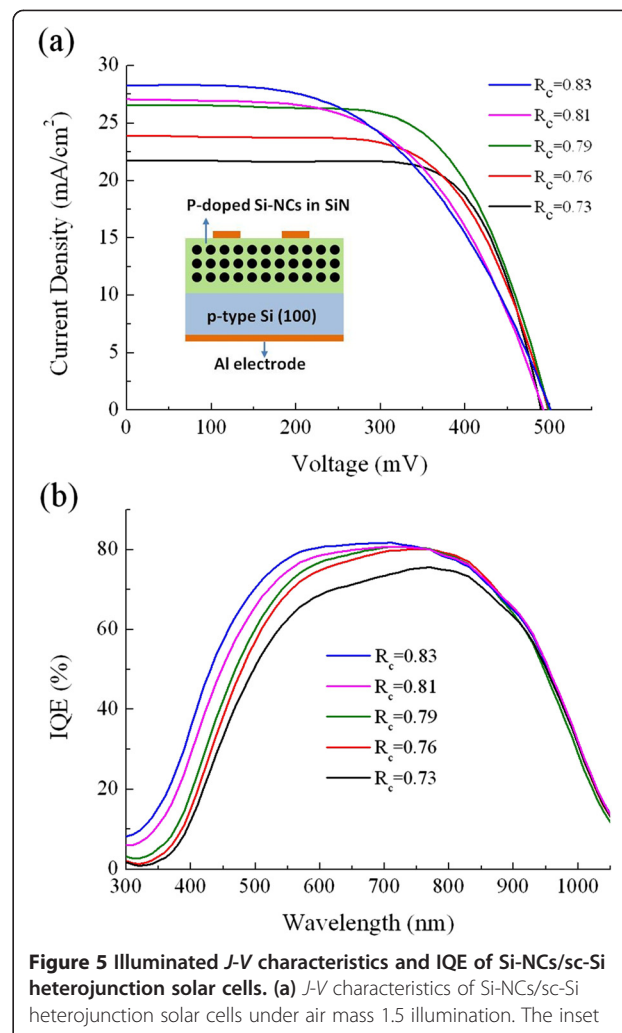
**Figure 3 Representative TEM image of the P-doped Si-NCs/Si<sub>x</sub> film with  $R_c = 0.79$ .** The crystalline structure of Si-NCs is circled by white circles. Dashed lines indicate interfaces between the Si-NCs/Si<sub>x</sub> film and surrounding c-Si wafer and epoxy layer.

on the integrated area under the N 1s, Si 2p, and P 2p peaks in conjunction with the sensitivity factors for the elements [16]. Figure 1a shows Si and P concentrations in the samples as a function of the  $R_c$  value. The Si concentration decreases from 70.8 to 62.9 atomic percent (at.%) with the  $N_2/\text{SiH}_4$  flow ratio adjusted from 0.73 to 0.83, while the P concentration is kept around 3 at.% since the  $\text{PH}_3/\text{SiH}_4$  flow ratio was kept constant during film growth. In order to obtain efficient carrier extraction, a photovoltaic device generally requires the presence of a p-n junction for carrier separation. Thus, active doping of phosphorus in Si-NCs is required for Si-NCs/sc-Si heterojunction solar cells. In this study, XPS was also used to study the chemical structure of P-doped SRN films after post-growth annealing. Figure 1b shows the Si 2p XPS spectrum of a representative SRN sample with  $R_c = 0.79$  after annealing. The deconvolution of the Si 2p signal consists of two peaks centered around 99.6 and 101.3 eV, which correspond to elemental Si and Si coordinated in the Si<sub>x</sub> network, respectively [17]. The analysis of the Si 2p peak indicates that the excess Si atoms precipitate out from the dielectric network, leading to the phase separation and formation of Si-NCs. The change in the XPS peak intensity ratio  $I_{\text{Si-Si}}/(I_{\text{Si-Si}} + I_{\text{Si-N}})$  was applied to investigate the influence of the N/Si ratio on the phase separation in annealed SRN films. As expected, the  $I_{\text{Si-Si}}/(I_{\text{Si-Si}} + I_{\text{Si-N}})$  decreases with increasing  $R_c$  value (shown in Figure 1c), implying that both phase separation and Si crystallization are reduced in the sample with a lower excess Si concentration.



The P 2p XPS signal of the annealed SRN film could be deconvoluted into two peaks centered around 129.2 and 130.3 eV (shown in Figure 1d), which are assigned to P atoms surrounded in part with Si atoms and pure phosphorous, respectively [17]. As depicted in Figure 1c, the value of  $I_{\text{Si-P}}/(I_{\text{Si-P}} + I_{\text{P-P}})$  decreases when increasing the N<sub>2</sub>/SiH<sub>4</sub> flow ratio. It is suggested that the concentration of the Si-P bond is proportional to the excess Si concentration, implying that phosphorus atoms may exist inside the Si-NCs or at the interfaces between Si-NCs and the SiN<sub>x</sub> matrix in the form of Si-P bonds.

Figure 2a shows the Raman spectra of the P-doped SRN films with various  $R_c$  values after annealing at 950°C for 30 min. The peak corresponding to the c-Si mode (located between 510 and 520 cm<sup>-1</sup>) appears due to precipitation of Si-NCs in the films during annealing. As depicted in Figure 2a, the growing c-Si peak intensity with decreasing  $R_c$  value indicates that the volume fraction of Si-NCs increases with increasing excess Si concentration in the SRN films, which is consistent with XPS results shown in Figure 1c. In this study, the average Si-NC size was estimated from the XRD data with the Scherrer



equation:  $D = k\lambda / \beta \cos\theta$ , where  $D$  is the average crystallite size,  $\lambda$  is the wavelength of the X-ray,  $\beta$  is the full width at half maximum (FWHM) of the diffraction peak, and  $\theta$  is the Bragg angle [18]. The value of the correction constant  $k$  was usually taken equal to 0.9 for Si. Figure 2b shows the average Si-NC size of the Si-NCs/SiN<sub>x</sub> film as a function of the  $R_c$  value. It is observed that the average crystallite size decreases from 7.3 to 3.0 nm for the Si-NCs/SiN<sub>x</sub> films over the investigated range of N<sub>2</sub>/SiH<sub>4</sub> flow ratio. High-resolution TEM was also used to confirm the formation of Si-NCs. Figure 3 shows a representative TEM image of the Si-NCs/SiN<sub>x</sub> film with  $R_c = 0.79$ . The lattice fringes in the amorphous SiN<sub>x</sub> matrix indicate the formation of Si-NCs. The size distribution of Si-NCs is in the range of 3 to 8 nm. The calculated average size of Si-NCs obtained from TEM images is consistent with that estimated from the XRD measurement.

In this work, the optical absorption of the P-doped Si-NCs/SiN<sub>x</sub> film was evaluated using optical gap E<sub>04</sub> defined as the energy at which the absorption coefficient is equal to 10<sup>4</sup> cm<sup>-1</sup>. In order to obtain the energy E<sub>04</sub>, the extinction coefficient was deduced from ellipsometry measurements, and then the absorption coefficient  $\alpha$  was calculated from the determined extinction coefficient  $k$  through the relation  $\alpha = 4\pi k / \lambda$ , where  $\lambda$  is the wavelength. Figure 4a shows absorption coefficients of the P-doped Si-NCs/SiN<sub>x</sub> films versus the incident photon energy. In addition, the electrical conductivity of the P-doped Si-NCs/SiN<sub>x</sub> film was measured by the van der Pauw method at room temperature. The derived optical gap E<sub>04</sub> and electrical conductivity are shown as a function of the N<sub>2</sub>/SiH<sub>4</sub> flow ratio in Figure 4b. As the nitrogen content increases, the electrical conductivity decreases from 46.4 to 6.7 S/cm over the investigated range of N<sub>2</sub>/SiH<sub>4</sub> ratio, while the opposite trend is observed for the optical gap E<sub>04</sub>, increasing with a gain of 0.52 eV. The Si-NCs/SiN<sub>x</sub> film is considered as a two-phase heterogeneous material, consisting of low-resistivity Si-NCs needed for good carrier transport and the wide bandgap SiN<sub>x</sub> matrix for high transparency. According to the effective medium approximation [19], the Si-NCs/SiN<sub>x</sub> film can be schematized as an effective medium, and its physical properties (electrical conductivity and absorption coefficient) could be derived from the physical properties and volume fractions of each phase. Thus, the less conductive and more transparent material obtained with increasing nitrogen content could be ascribed to the reduction in volume fraction of Si-NCs, as depicted in Figure 2a. In addition, due to the quantum confinement effects [20], the shrinkage of the Si-NC size with increasing R<sub>c</sub> value may result in bandgap expansion, which also leads to an increase in the effective optical gap of the Si-NCs/SiN<sub>x</sub> film.

The P-doped Si-NCs/SiN<sub>x</sub> layers with various R<sub>c</sub> values were fabricated on top of p-type sc-Si substrates for fabrication of Si heterojunction solar cells, as shown in the inset of Figure 5a. This study concentrates on basic Si-NCs/sc-Si heterojunction solar cells without the designs or processes to enhance the conversion efficiency, such as surface texturing, anti-reflection coating and back-surface field. The illuminated J-V curves corresponding to each sample are displayed in Figure 5a, and their open-circuit voltage (V<sub>oc</sub>), short-circuit current density (J<sub>sc</sub>), fill factor (FF), and efficiency are shown in Figure 6 as a function of the N<sub>2</sub>/SiH<sub>4</sub> flow ratio. The magnitude of V<sub>oc</sub> is generally correlated to the built-in potential (V<sub>bi</sub>) of the junction, which could be influenced by the energy bandgap of the Si-NCs for the Si heterojunction solar cells. As shown in Figure 7, the V<sub>bi</sub> of the P-doped Si-NCs/sc-Si heterojunction extracted from the capacitance-voltage characteristic increases from 0.77 to 1.95 V with increasing R<sub>c</sub> value. This trend may be ascribed to the

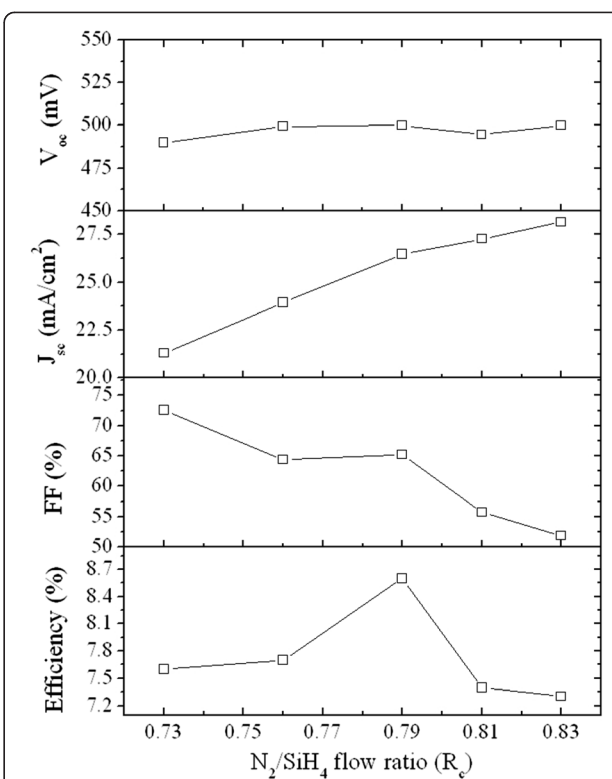


**Figure 6** One-sun illuminated cell parameters of Si-NCs/sc-Si heterojunction solar cells. The V<sub>oc</sub>, J<sub>sc</sub>, FF, and efficiency of the fabricated Si-NCs/sc-Si heterojunction cells with different R<sub>c</sub> values.

bandgap expansion of Si-NCs with the shrinkage of the Si-NC size, leading to an increase in V<sub>bi</sub> at the junction, and thus, the Si heterojunction solar cell is expected to show a higher V<sub>oc</sub> as R<sub>c</sub> increases. However, in this study, the V<sub>oc</sub> value is in the range of 0.49 to 0.5 for all Si heterojunction solar cells (shown in Figure 6).

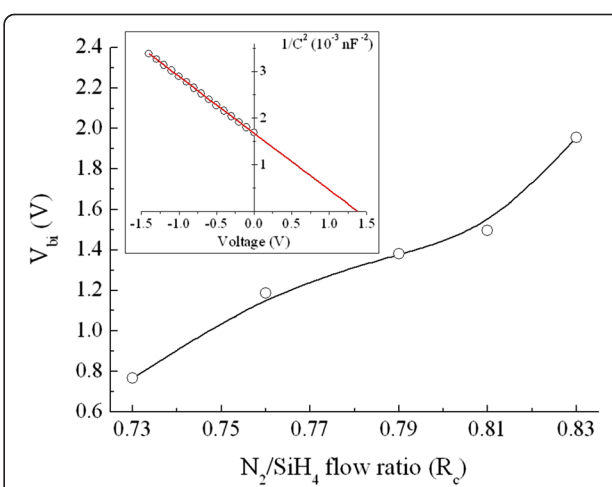


**Figure 7** Built-in potential of the Si-NCs/sc-Si heterojunction as a function of the R<sub>c</sub> value. The inset is an inverse capacitance-square plot of the R<sub>c</sub> = 0.79 sample.

implying that  $V_{oc}$  is quite insensitive to the Si-NC size. Figure 8 shows dark  $J-V$  curves for the solar cells with different  $R_c$  values. Both the saturation current density ( $J_0$ ) and the ideality factor ( $n$ ) were extracted by fitting the dark  $J-V$  curves at intermediate voltages (approximately 0.4 to 0.5 V) using a diode equation  $J = J_0 \exp(qV/nkT)$ , where  $q$  is the electron charge,  $T$  is the temperature, and  $k$  is the Boltzmann constant [21]. As shown in the inset of Figure 8, the values of  $J_0$  and  $n$  are in the ranges of  $1.5 \times 10^{-6}$  to  $5 \times 10^{-6} \text{ A/cm}^2$  and 2.5 to 3 for all heterojunction solar cells, respectively. The large  $n$  value ( $n > 2$ ), together with the high  $J_0$ , indicates that the recombination current contributes significantly to the conduction process in the cells, which may be caused by trap-assisted tunneling or field-assisted recombination at point defects [22,23]. It has been reported that formation of charged defects would occur in  $\text{SiN}_x$  films after high-temperature annealing owing to the removal of hydrogen atoms [24,25]. Since the charged defect density in the annealed film should be proportional to the volume fraction of the  $\text{SiN}_x$  matrix, we suggest that the increase in the charge defect density would increase the probability of trap-assisted tunneling and thus compensate the enhanced  $V_{bi}$  effect with increasing  $R_c$  value, leading to similar  $J_0$ , as well as  $V_{oc}$  for all heterojunction solar cells.

From Figure 6, the  $J_{sc}$  is increased from 21.3 to  $28.2 \text{ mA/cm}^2$  with increasing  $R_c$  value. This trend could be ascribed to the lower parasitic absorption in the Si-NCs/ $\text{SiN}_x$  film with a higher  $R_c$  value since the increasing Si-NC phase could result in a reduction in the optical gap of the film due to its higher absorption coefficient, as mentioned above (see Figure 4b). To better understand the difference in  $J_{sc}$  among the heterojunction solar cells with various  $R_c$  values, losses of the  $J_{sc}$  in the devices were investigated from their IQE data by spectral response measurements. As shown in Figure 5b, the heterojunction

device with a higher  $R_c$  Si-NCs/ $\text{SiN}_x$  film shows a higher IQE in the short wavelength regime, especially for the wavelength range between 400 and 700 nm, while the IQE spectra in the infrared wavelength regime ( $>900 \text{ nm}$ ) are similar for all heterojunction solar cells, implying that recombination of photo-generated charge carriers in the absorber layer is almost the same in all heterojunction devices [26]. Moreover, as depicted in Figure 4a, the obvious variations in the absorption spectra of the P-doped Si-NCs/sc-Si films with various  $R_c$  values could be observed at photon energies above 1.8 eV (approximately  $<700 \text{ nm}$ ), which shows good correspondence with the trends in the IQE data. Therefore, it is speculated that the difference in  $J_{sc}$  losses among the devices could be attributed to the parasitic absorption in the emitter layer. More photons in the visible spectrum would be absorbed with increasing volume fraction of the Si-NCs in the P-doped Si-NCs/sc-Si film, leading to the limitation in the available solar spectrum in the device, as well as the degradation of the  $J_{sc}$ .

In contrast to the  $J_{sc}$ , the FF decreases from 72.6% to 51.9% when increasing the  $R_c$  value, as depicted in Figure 6. The series resistance ( $R_s$ ) of the Si heterojunction solar cell was extracted from the dark  $J-V$  characteristic and shown in Figure 9 as a function of the  $R_c$  value. The fill factor of a solar cell depends upon the series resistance, saturation current density, and diode ideality factor. Here, the reduction in FF with increasing  $R_c$  value could be mainly attributed to an increase in  $R_s$  since the values of  $J_0$  and  $n$  are similar for all heterojunction solar cells, as shown in the inset of Figure 8. As depicted in Figure 9, the  $R_s$  of the Si heterojunction solar cell is highly correlated to the conductivity of the P-doped Si-NCs/sc-Si film. Thus, it could be speculated that the FF of the Si heterojunction solar cell strongly depends on the conductivity of the P-doped Si-NCs/ $\text{SiN}_x$  film. The maximum conversion efficiency is achieved from the device with  $\text{N}_2/\text{SiH}_4$  ratio of 0.79 (shown in Figure 6),

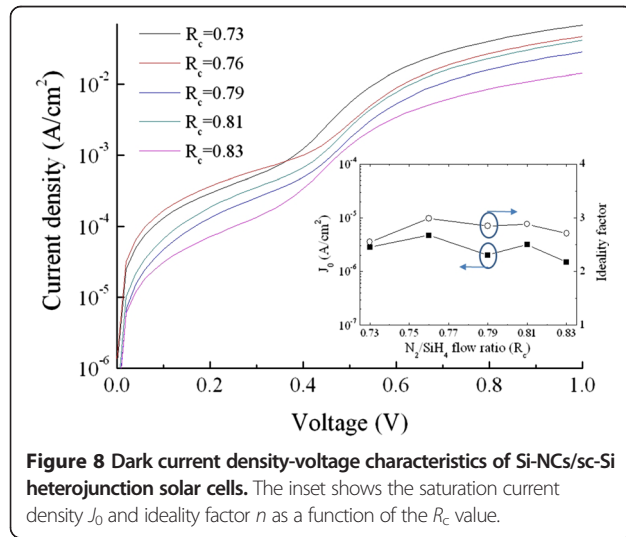


**Figure 8** Dark current density-voltage characteristics of Si-NCs/sc-Si heterojunction solar cells. The inset shows the saturation current density  $J_0$  and ideality factor  $n$  as a function of the  $R_c$  value.

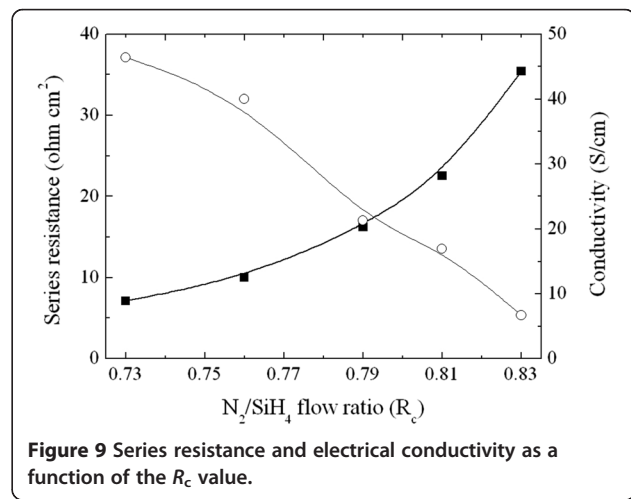


**Figure 9** Series resistance and electrical conductivity as a function of the  $R_c$  value.

where the balance between  $J_{sc}$  and FF losses is optimized. The best heterojunction solar cell has 8.6% conversion efficiency, with a  $V_{oc}$  of 500 mV,  $J_{sc}$  of  $26.5 \text{ mA/cm}^2$ , and 65.2% in fill factor. While the data obtained is based on our preliminary fabrication of Si-NCs/sc-Si heterojunction cells, further improvement in fabrication of Si-NC emitters (layer thickness, deposition and doping conditions, etc.) and related process parameters is likely to improve the photovoltaic efficiency.

## Conclusions

In this report, we have investigated the feasibility of using P-doped Si-NCs/SiN<sub>x</sub> films as emitters on p-type sc-Si substrates for fabrication of Si-based heterojunction solar cells. From XPS analysis of the P-doped Si-NCs/SiN<sub>x</sub> films, the P 2p signal only attributed to Si-P or P-P bonds indicates that the P atoms may exist inside Si-NCs. The electrical and optical properties of the P-doped Si-NCs/SiN<sub>x</sub> material are strongly influenced by its chemical composition (N/Si ratio). The optical gap  $E_{04}$  is enhanced with increasing nitrogen content, while the conductivity is deteriorated. These trends could be interpreted by a bi-phase model, where the SiN<sub>x</sub> phase contributes to the optical gap enhancement and the Si-NC phase promotes charge carrier transport. Therefore, the  $J_{sc}$  is increased with increasing N/Si ratio in the Si-NCs/SiN<sub>x</sub> layer, while the FF is reduced. The best cell parameters obtained are  $V_{oc}$  of 500 mV,  $J_{sc}$  of  $28.2 \text{ mA/cm}^2$ , FF of 65.2%, and conversion efficiency of 8.6% from the heterojunction solar cell with a  $R_c = 0.79$  Si-NCs/SiN<sub>x</sub> emitter. Further device optimization is required to improve the photovoltaic efficiency.

## Competing interests

The authors declare that they have no competing interests.

## Authors' contributions

PJW carried out the material and device preparation and drafted the manuscript. YCW carried out the material and device characterization. ICC conceived of the study and participated in its design and coordination. All authors read and approved the final manuscript.

## Acknowledgements

This research was supported by the National Science Council of Taiwan under grant nos. 101-2221-E-008-041 and 101-2622-E-008-015-CC3.

Received: 2 June 2013 Accepted: 26 October 2013

Published: 5 November 2013

## References

- Cho E-C, Park S, Hao X, Song D, Conibeer G, Park S-C, Green MA: Silicon quantum dot/crystalline silicon solar cells. *Nanotechnology* 2008, **19**:245201.
- Park S, Cho E, Song D, Conibeer G, Green MA: n-Type silicon quantum dots and p-type crystalline silicon heteroface solar cells. *Sol Energy Mater Sol Cells* 2009, **93**:684–690.
- Hong SH, Kim YS, Lee W, Kim YH, Song JY, Jang JS, Park JH, Choi S-H, Kim KJ: Active doping of B in silicon nanostructures and development of a Si quantum dot solar cell. *Nanotechnology* 2011, **22**:425203.
- Perez-Wurfl I, Ma L, Lin D, Hao X, Green MA, Conibeer G: Silicon nanocrystals in an oxide matrix for thin film solar cells with 492 mV open circuit voltage. *Sol Energy Mater Sol Cells* 2012, **100**:65–68.
- Conibeer G, Green M, Cho E-C, König D, Cho Y-H, Fangsuwannarak T, Scardera G, Pink E, Huang Y, Puzzer T, Huang S, Song D, Flynn C, Park S, Hao X, Mansfield D: Silicon quantum dot nanostructures for tandem photovoltaic cells. *Thin Solid Films* 2008, **516**:6748–6756.
- Hao XJ, Podhorodecki AP, Shen YS, Zatryb G, Misiewicz J, Green MA: Effect of Si-rich oxide layer stoichiometry on the structure and optical properties of Si-QD/SiO<sub>2</sub> multilayer films. *Nanotechnology* 2009, **20**:485703.
- Daldozzo N, Das G, Larcheri S, Mariotto G, Dalba G, Pavesi L, Irrera A, Priolo F, Iacona F, Rocca F: Silicon nanocrystal formation in annealed silicon-rich silicon oxide films prepared by plasma enhanced chemical vapor deposition. *J Appl Phys* 2007, **101**:113510.
- Singh SP, Srivastava P, Ghosh S, Khan SA, Prakash GV: Phase stabilization by rapid thermal annealing in amorphous hydrogenated silicon nitride film. *J Phys Condens Matter* 2009, **21**:095010.
- Delachat F, Carrada M, Ferblantier G, Grob J-J, Slaoui A: Properties of silicon nanoparticles embedded in SiN<sub>x</sub> deposited by microwave-PECVD. *Nanotechnology* 2009, **20**:415608.
- Wan Z, Huang S, Green MA, Conibeer G: Rapid thermal annealing and crystallization mechanisms study of silicon nanocrystal in silicon carbide matrix. *Nano Res Lett* 2011, **6**:129.
- Cheng QJ, Tam E, Xu S, Ostrikov K: Si quantum dots embedded in an amorphous SiC matrix: nanoparticle control by non-equilibrium plasma hydrogenation. *Nanoscale* 2010, **2**:594–600.
- Feroughi OM, Sternemann C, Sahle CJ, Schroer MA, Sternemann H, Conrad H, Hohl A, Seidler GT, Bradley J, Fister TT, Balasubramanian M, Sakk A, Pirkkalainen K, Hamalainen K, Tolan M: Phase separation and Si nanocrystal formation in bulk SiO studied by X-ray scattering. *Appl Phys Lett* 2010, **96**:081912.
- Hao XJ, Cho E-C, Flynn C, Shen YS, Park SC, Conibeer G, Green MA: Synthesis and characterization of boron-doped Si quantum dots for all-Si quantum dot tandem solar cells. *Sol Energy Mater Sol Cells* 2009, **93**:273–279.
- Ma L, Lin D, Conibeer G, Perez-Wurfl I: Introducing dopants by diffusion to improve the conductivity of silicon quantum dot materials in 3rd generation photovoltaic devices. *Phys Stat Sol c* 2011, **8**:205–208.
- Zacharias M, Heitmann J, Scholz R, Kahler U, Schmidt M, Bläsing J: Size-controlled highly luminescent silicon nanocrystals: a SiO/SiO<sub>2</sub> superlattice approach. *Appl Phys Lett* 2002, **80**:661–663.
- Moulder JF, Stickle WF, Sobol PE, Bomben KD: *Handbook of X-ray Photoelectron Spectroscopy*. Eden Prairie: Perkin-Elmer Corp, Physical Electronics Division; 1995.
- Wu PJ, Wang YC: Chen IC: Influence of phosphorous doping on silicon nanocrystal formation in silicon-rich silicon nitride films. *J Phys D Appl Phys* 2013, **46**:125104.
- Cullity BD, Stock SR: *Elements of X-Ray Diffraction*. Upper Saddle River: Prentice-Hall; 2001.
- Stroud D: The effective medium approximations: some recent developments. *Superlattice Microstruct* 1998, **23**:567–573.
- Kim TW, Cho CH, Kim BH, Park SJ: Quantum confinement effect in crystalline silicon quantum dots in silicon nitride grown using SiH<sub>4</sub> and NH<sub>3</sub>. *Appl Phys Lett* 2006, **88**:123102.
- Fujiwara H, Kondo M: Effects of aSi:H layer thicknesses on the performance of aSi:H/CsI heterojunction solar cells. *J Appl Phys* 2007, **101**:054516.
- Kaminski A, Marchand JJ, Laugier A: Non ideal dark I-V curves behavior of silicon solar cells. *Sol Energy Mater Sol Cells* 1998, **51**:221–231.
- Breitenstein O, Bauer J, Lotnyk A, Wagner JM: Defect induced non-ideal dark I-V characteristics of solar cells. *Superlattices Microstruct* 2009, **45**:182–189.
- Sahu BS, Delachat F, Slaoui A, Carrada M, Ferblantier G, Muller D: Effect of annealing treatments on photoluminescence and charge storage mechanism in silicon-rich SiN<sub>x</sub>H films. *Nano Res Lett* 2011, **6**:178.
- De Wolf S, Agostinelli G, Beaumé G, Vitanov P: Influence of stoichiometry of direct plasma-enhanced chemical vapor deposited SiN<sub>x</sub> films and silicon substrate surface roughness on surface passivation. *J Appl Phys* 2005, **97**:063303.
- Jensen N, Hausner RM, Bergmann RB, Werner JH, Rau U: Optimization and characterization of amorphous/crystalline silicon heterojunction solar cells. *Prog Photov Res Appl* 2002, **10**:1–13.

doi:10.1186/1556-276X-8-457

**Cite this article as:** Wu et al.: Fabrication of Si heterojunction solar cells using P-doped Si nanocrystals embedded in SiN<sub>x</sub> films as emitters. *Nanoscale Research Letters* 2013 **8**:457.